Programmable color tuning of a multiline laser by means of a twisted nematic liquid crystal display

José Luis Martínez,[1] María del Mar Sánchez-López,[2] Pascuala García-Martínez,[3] Ignacio Moreno,[1,*] and Juan Campos[4]

[1]Departamento de Ciencia de Materiales, Óptica y Tecnología Electrónica, Universidad Miguel Hernández, Elche 03202, Spain

[2]Instituto de Bioingeniería, Universidad Miguel Hernández, Elche 03202, Spain

[3]Departament d'Òptica, Universitat de València, C/Doctor Moliner 50, Burjassot 46100, Spain

[4]Departamento de Física, Universitat Autònoma de Barcelona, Bellaterra 08193, Spain

*Corresponding author: i.moreno@umh.es

Received 3 May 2012; revised 26 July 2012; accepted 3 August 2012;
posted 3 August 2012 (Doc. ID 167910); published 10 September 2012

An optical system useful to tune in a controlled way the color of a triline argon krypton (Ar–Kr) laser by means of a twisted nematic liquid crystal display (TNLCD) is presented. The optical setup employs a 4*f* system and two blazed gratings to first separate and then recombine the spectrum of the light beam. The TNLCD is included in the intermediate focal plane operating in the amplitude modulation mode to control the relative transmission of each spectral line. The resulting color is accurately predicted by using a previously developed physical model of the spectral and voltage dependence of the TNLCD birefringence. By simply changing the gray level image addressed to the display, the Ar–Kr laser is color modulated at a video rate, thus becoming an interesting, reconfigurable, coherent light source for applications such as multicolor holography or color inspection.

OCIS codes: 070.6120, 230.3720, 070.2615.

1. Introduction

Nowadays, liquid crystal displays (LCD) play a relevant role in many types of optical devices and systems [1]. While their primary application is as image-displaying elements, there are a number of other uses in areas like diffractive optics, polarization optics, and adaptive optics where the possibility to program an optical element opens a widespread number of applications where reconfigurable optical elements are incorporated onto the LCD. Therefore, LCDs play an important role as spatial light modulators (SLM) and have become typical devices in research laboratories in these fields.

Usually, LCD monitors employ white light illumination. Color management is achieved by dividing each pixel into three subpixels with RGB color filters where each individual color component of the image is addressed to the corresponding pixels [2]. Alternatively, LCD-based projection displays typically achieve color reproduction by means of three independent LCD microdisplays illuminated with red, green, and blue primary spectra extracted from a single white light with passband filters [3]. They may also achieve color reproduction by using a single microdisplay that sequentially displays the RGB components synchronized with a corresponding temporal sequence of illumination with red, green, and blue light [4]. This temporal illumination sequence is typically obtained by means of filtering optical disks or with switchable LED sources.

However, the dispersion characteristics of the liquid crystal layer leads to some degree of color modulation when it is directly illuminated with white light (no passband filters are included) and it is

1559-128X/12/266368-08$15.00/0

inserted between linear polarizers [5,6]. In fact, this arrangement resembles the basic element of well-known polarization interference filters whose operation is based on the dispersion characteristics and polarization transformation properties of wave plates [1]. The fact that the phase shift of a liquid crystal wave plate can be voltage controlled prompted their use in building tunable polarization interference filters. For instance, such a filter based on the classical Lyot design was reported in [7] for multispectral color capturing. There, a liquid crystal cell replaced each wave plate in order to allow phase shift control by means of an electric signal. Those filters are commonly calibrated in applications requiring high accurate spectral or colorimetric measurements such as multispectral imaging acquisition [8] or diffractive optical elements with chromatic control [9]. However, liquid crystal tunable polarization filters suffer from low overall intensity transmission due to the great number of elements primarily required for short visible wavelengths. Moreover they are not useful to produce a wide color gamut since the transmission band is narrow around the central wavelength.

In this paper we achieve color control of a laser source by modifying an optical architecture that we borrowed from another well-established application of LCD microdisplays such as ultrashort pulse shaping [10]. In such systems, the input light is angularly dispersed by a prism or a diffraction grating. A 4*f* Fourier transform optical system is adapted so that each spectral component is focused onto a different spatial location in the Fourier plane. A spatially patterned mask is displayed on the LCD then modulates the phase and amplitude of the spatially dispersed spectral components. After the spectral components are recombined by a second lens and grating, a shaped output pulse is obtained. Note that the optical system is equivalent to that used in Fourier transform spectrometers where LCDs have also been employed as spatial light modulator masks [11]. Related architectures have been extensively used in wavelength division multiplexing (WDM) systems [12], and recently such systems were demonstrated with a liquid crystal on silicon (LCoS) phase modulator incorporated [13]. While liquid crystal systems usually manage spectral ranges in the close infrared range for applications in optical communications, in this work, we are interested in modulating the color of a multiline white visible laser source. We adopt the above-mentioned optical architecture to adjust the relative transmission of the spectral components of such a laser source with the goal of controlling, at the video rate, the color of such coherent light beams.

The generation of laser light in the three primary-color region is an interesting subject not only for laser physics, but also for technological applications such as illumination, multicolor laser sensing, and so on. Semiconductor laser diodes are ideal sources for RGB applications thanks to their continuing volume and cost reduction [14]. However, ion lasers such as He–Cd, Ar–Kr, and dye-mixture lasers are also well known and in general more powerful multicolor lasers [15] that, in addition, do no require alignment. However, the intensity of their individual wavelength emissions can not be independently controlled and, in many cases, the efficiency is low. One very interesting application of such lasers is multicolor computer generated holography, where RGB components of digital holograms are illuminated with the corresponding color light. White RGB lasers can be used for that purpose, together with color selective filters and stacked holograms [16,17]. In other cases, a spatial light modulator has been used to time multiplex the displayed RGB computer generated holograms in conjunction with commuted light sources that can be either a filtered white laser [4], an aligned laser [18], or LED systems [19]. A color laser source which color can be completely controlled could be useful for such applications.

Here we investigate the multicolor generation by externally tuning the transmission of the three primary lines emitted by a white ion Ar–Kr laser that are employed as the primary colors. For that purpose we use the above-mentioned optical system using a twisted nematic LCD (TNLCD) acting as a spatial light modulator in the Fourier plane of a 4*f* system. The TNLCD is operated in an intensity modulation configuration in order to control the spectral transmittance by simply changing the image addressed to the display at video rate. To properly operate the TNLCD, a good knowledge of the physical parameters affecting its optical modulation, typically the orientation of the liquid crystal director and the birefringence, is required. Since this information is not usually available in commercial displays, a number of reverse engineering experiments have been proposed in the literature to measure such parameters prior to selecting the appropriate polarization configuration [20]. The characteristic chromatic dispersion of the liquid crystal birefringence makes these display parameters wavelength dependent [21]. The chromatic dispersion is also the reason why the phase modulation depth provided by LCDs is very dependent on the wavelength, showing larger phase values for shorter wavelengths [22]. Here we use a relatively simple physical model of the TNLCD spectral retardance that has been probed to provide very accurate predictions of the complex amplitude [20], spectral [21] and color [6] modulation characteristics of a number of commercial devices. In these previous works, the display was homogeneously illuminated with all spectral components of a white light bulb with continuous spectrum. Therefore, a limited color modulation range was obtained. Here, on the contrary, we use the above mentioned 4*f* system to spatially separate the spectral components on the screen of the TNLCD display, therefore allowing a modulation to each component separately. The color of the laser beam obtained once the spectral components are recombined can be accurately selected. Colorimetric measurements in the chromatic diagram

are presented and show the wide color gamut that can be generated with the proposed system.

The paper is organized as follows. In Section 2 we briefly review the Jones matrix TNLCD retardance model used to obtain the spectral intensity modulation of the device. In Section 3 we describe the optical setup we have used to individually modulate the intensity of each spectral component and how the colorimetric properties of the system's output beams are derived from the previous model. The experimental results showing the color tuning characteristics of the laser beam are presented in Section 4. Finally, Section 5 contains the conclusions of the work.

2. Jones Matrix Model of the TNLCD Spectral Intensity Modulation

The employed physical model was initially proposed in [20]. It considers that the TNLCD cell is characterized by three parameters: (1) the twist angle (α), (2) the effective retardance (β) introduced by the liquid crystal layers in the central region of the cell that is considered to have a linear twist-angle variation and also a uniform tilt angle that depends on the applied voltage, and (3) the effective retardance (δ) introduced by the edge (boundary) liquid crystal layers where the liquid crystal director is unable to tilt. The Jones matrix $\mathbf{M_{LCD}}$ describing the LCD is given by [20]:

$$\mathbf{M_{LCD}}(\alpha,\beta,\delta) = e^{-i(\beta+2\delta)}\mathbf{R}(-\alpha)\cdot\mathbf{M}(\alpha,\beta,\delta), \tag{1}$$

where $\mathbf{R}(-\alpha)$ is the 2×2 rotation matrix

$$\mathbf{R}(-\alpha) = \begin{pmatrix} \cos(\alpha) & -\sin(\alpha) \\ \sin(\alpha) & \cos(\alpha) \end{pmatrix}, \tag{2}$$

and the matrix $\mathbf{M}(\alpha,\beta,\delta)$ is given by

$$\mathbf{M}(\alpha,\beta,\delta) = \begin{pmatrix} A-iB & C \\ -C & A+iB \end{pmatrix}, \tag{3}$$

with

$$A = \cos(\gamma)\cos(2\delta) - \frac{\beta}{\gamma}\sin(\gamma)\sin(2\delta), \tag{4a}$$

$$B = \cos(\gamma)\sin(2\delta) + \frac{\beta}{\gamma}\sin(\gamma)\cos(2\delta), \tag{4b}$$

$$C = \frac{\alpha\,\sin(\gamma)}{\gamma}, \tag{4c}$$

$$\gamma = \sqrt{\alpha^2+\beta^2}. \tag{4d}$$

The Jones matrix in Eq. (1) corresponds to the reference framework where the liquid crystal director at the entrance surface of the display is considered parallel to the x axis (light propagation is along z axis). While the twist angle α is a constant value, the two retardance parameters β and δ are both voltage and wavelength sensitive. Typically, the voltage applied to the display is controlled via the computer graphic card, being determined by the addressed gray level (g), which ranges from 0 to 255.

A method for obtaining the effective retardance functions $\beta(\lambda,g)$ and $\delta(\lambda,g)$ was reported in [18], leading to a full prediction of the normalized spectral transmission function $\tau(\lambda,g)$ when the TNLCD is located between two linear polarizers, with orientations φ_1 and φ_2 relative to the x axis. The standard Jones calculus leads to the following relationship:

$$\begin{aligned}\tau(\lambda,g) = {} & [A(\lambda,g)\cos(\varphi_1-\varphi_2+\alpha) \\ & + C(\lambda,g)\times\sin(\varphi_1-\varphi_2+\alpha)]^2 \\ & + [B(\lambda,g)\times\cos(\varphi_1+\varphi_2-\alpha)]^2,\end{aligned} \tag{5}$$

where the wavelength and gray level dependence of $\beta(\lambda,g)$ and $\delta(\lambda,g)$ have been incorporated through Eqs. (1)–(4). Using this equation, it is possible to select the angles of the polarizers (φ_1, φ_2) that lead to an intensity modulation curve with maximum modulation range for the selected wavelengths, and adjust the addressed gray level to achieve a desired transmission intensity for a specific wavelength.

3. Optical Setup and Colorimetric Prediction

Considering the previous model, we now describe the experimental setup we have employed to modulate the intensity of each spectral component of a multiline laser source, and how the colorimetric content of the light transmitted by this setup can be derived.

Figure 1 shows the proposed optical setup. We employ an Ar–Kr ion laser (Melles-Griot, 35-LTL-835-240) as an illumination source that simultaneously emits three laser lines at 647, 568, and 488 nm. Because of their color, these lines will be denoted henceforth as R, G, and B, respectively. A blazed transmission grating (Edmund, NT49-584), with 600 grooves/mm is used to angularly disperse the three spectral lines of the laser beam. The grating nominal diffraction efficiency exceeds 45% for the three selected wavelengths. Then, the beam on the first diffraction order is collimated by an achromatic

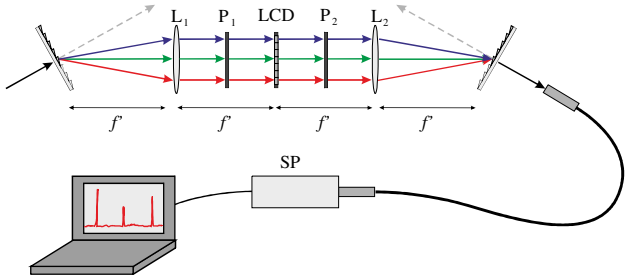

Fig. 1. (Color online) Scheme of the optical setup. L denotes converging lenses, P denotes linear polarizers, LCD the liquid crystal display, and SP the spectrometer.

doublet lens, with 10 cm focal lens, and the TNLCD is placed at the lens back focal plane. Two linear polarizers are placed on each side of the display in order to select the appropriate polarization configuration to achieve an intensity modulation response. An inverse symmetric optical system is built with an equivalent lens and an equivalent blazed grating. The three laser components are then recombined on the first diffraction order of this second grating. This recombined beam is analyzed with a calibrated Stellar-Net portable spectrometer, model EPP-2000.

Figure 2(a) shows the diffraction pattern generated after the first blazed grating when it is illuminated with the Ar–Kr laser. Note that a blazed grating illuminated with the design wavelength diffracts all the light to the $+1$ order. However, when illuminated with other wavelengths, the diffraction efficiency decreases and other orders are also present. In the zero order the spectral components are not separated, and therefore the white laser beam can be appreciated. The three spectral components of the laser are separated on the ± 1 diffraction order showing better efficiency at the positive order. In order to avoid saturation of the CCD camera, this picture has been taken with the laser at the minimum power that emits all three laser lines and shows that the blue line is the most intense while the red one is the weakest. However, the power of the laser beam can be varied in a certain range where the intensity of the R, G, and B spectral components is, in general, not equal. In our experiments the input power is adjusted to provide enough light emission in all three lines. This input power function is selected as the reference incident laser spectrum as $i(\lambda)$. Figure 2(b) shows the spectrometer measurement of the recombined laser beam, showing the three line spectral irradiance, that can be approximated as

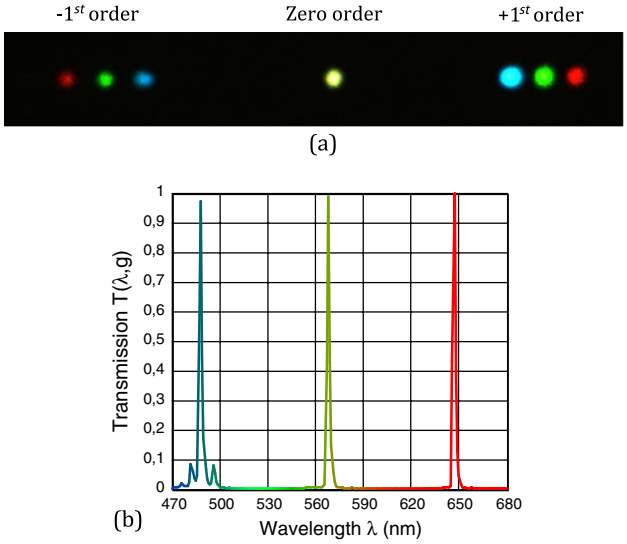

Fig. 2. (Color online) Experimental spectrum of the input light beam. (a) Picture of the diffraction pattern after the blazed grating and (b) measurement of the recombined beam spectrum with the spectrometer after adjusting the power input.

$$i(\lambda) \cong \sum_{i=\mathrm{R,G,B}} c_i \delta(\lambda - \lambda_i), \tag{6}$$

where c_i are coefficients that account for the relative intensity of each RGB laser line. $\delta(\cdot)$ is the Dirac delta function.

We employed a commercial TNLCD spatial light modulator from CRL-Opto, model XGA-3, with 1024 pixels × 768 pixels, with a measured twist angle $\alpha = -94°$. Maximum voltage is applied to the device for gray level $g = 0$, and it decreases as g increases. The retardance parameters were measured as a function of g and λ as reported earlier [20,21]. Figure 3 shows the dependence of these parameters with the addressed gray level for the three Ar–Kr laser wavelengths. Although the values $\delta(\lambda, g)$ corresponding to the retardance introduced by the edge liquid crystal layers are rather small, they should not be neglected since they remarkably contribute to achieve accurate predictions of the optical modulation. Since we are interested in modulating the color of the recombined laser beam as shown in Fig. 1, we seek a configuration of the polarizers that yields a wide variation of the intensity modulation curve for each spectral component, but most importantly, it yields very good null transmission for the three of them. In this way, the system can lead to highly saturated colors of the final recombined light beam, since the three primary wavelengths can be effectively eliminated. Therefore, we applied Eq. (5) and the data in Fig. 2 to predict the normalized intensity transmission for the three RGB wavelengths and for different orientations φ_1 and φ_2 of

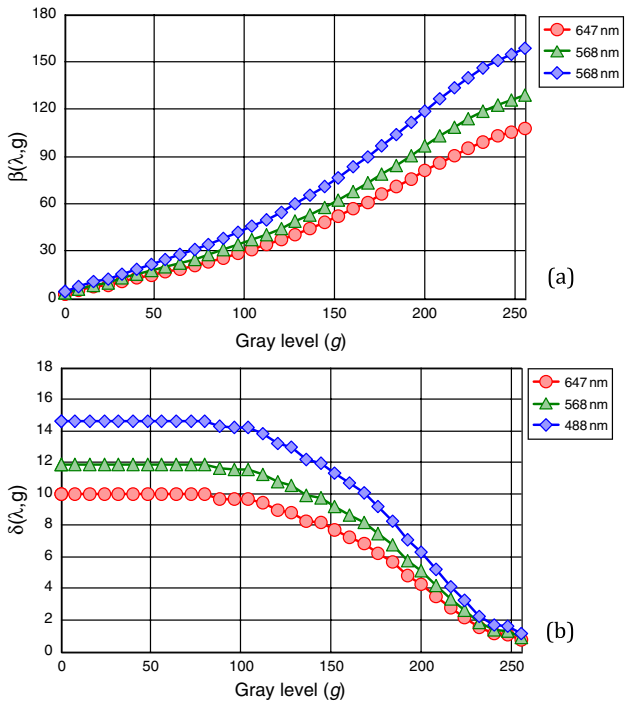

Fig. 3. (Color online) TNLCD effective retardance parameters β and δ, in degrees, as a function of the addressed gray level, for the three RGB wavelengths.

the two polarizers. The best results were obtained for $\varphi_1 = 42°$ and $\varphi_2 = -48°$. Note that the input polarizer can additionally reduce efficiency if its orientation does not coincide with the input laser polarization. However, an achromatic half-wave plate could be added to reorient the input polarization. Figure 4 shows the intensity transmission as a function of the addressed gray level for the RGB wavelengths for this configuration. The continuous lines correspond to the predicted numerical transmission, while the points in the curves are the corresponding experimental data. The agreement between the numerical and the experimental results is remarkable, thus confirming the excellent predictive properties of the liquid crystal physical model we are using.

Note the importance of using such a predictive physical model in order to be able to rapidly find a useful configuration adjusted for any optical experiment. For instance, as the first step, we finely adjusted the input power and the initial gray levels addressed to the LCD to provide three spectral lines with equal irradiance. This is indeed the spectrometer measurement shown in Fig. 2(b), which we will consider as the reference white laser beam. Note that the requirement of attenuating the blue line in comparison to the red one reduces the transmission dynamic range that can be applied to this component. However, the limited range is still enough to show complete color modulation.

The output spectral irradiance of the recombined laser beam $T(\lambda)$ is numerically calculated by multiplying the original laser spectrum, $i(\lambda)$, in Fig. 2(b) by the spectral transmittance curves $\tau(\lambda, g)$ for the selected polarizers configuration (curves in Fig. 4), namely

$$T(\lambda) = \tau(\lambda, g) i(\lambda). \tag{7}$$

As mentioned above, the intensity transmission $\tau(\lambda, g)$ of each RGB component can be adjusted with the proper addressed gray level. For that purpose, a gray level image is designed with three rectangular areas, each laser line impinging on the TNLCD over each of these three panel zones. A gray level vector $\hat{g} = (g_R, g_G, g_B)$ is defined whose components correspond to the gray level g_i applied to each spectral line. Therefore, the spectrum of the recombined light beam can be expressed as

$$T(\lambda) \cong \sum_{i=\mathrm{R,G,B}} c_i \tau_i \delta(\lambda - \lambda_i), \tag{8}$$

where $\tau_i \equiv \tau(\lambda_i, g_i)$ is the normalized transmission of the TNLCD for each spectral line. The addressed gray level g_i can be adjusted in each of these three areas in order to achieve a desired transmission intensity for each spectral line λ_i.

The color of the recombined output beam can be now determined by projecting the output spectral irradiance function in Eqs. (7) and (8) onto the basis of the color matching functions. As defined by the CIE 1931-XYZ standard observer, the tristimulus values of the transmitted light can be calculated as [23]:

$$X = \int_0^\infty T(\lambda)\bar{x}(\lambda)\mathrm{d}\lambda, \qquad Y = \int_0^\infty T(\lambda)\bar{y}(\lambda)\mathrm{d}\lambda,$$
$$Z = \int_0^\infty T(\lambda)\bar{z}(\lambda)\mathrm{d}\lambda. \tag{9}$$

Since we are considering a discrete spectrum with only three wavelengths, then

$$X(\hat{g}) = \sum_{i=\mathrm{R,G,B}} c_i \tau_i \bar{x}_i, \qquad Y(\hat{g}) = \sum_{i=\mathrm{R,G,B}} c_i \tau_i \bar{y}_i,$$
$$Z(\hat{g}) = \sum_{i=\mathrm{R,G,B}} c_i \tau_i \bar{z}_i, \tag{10}$$

where $\bar{x}_i \equiv \bar{x}(\lambda_i)$, $\bar{y}_i \equiv \bar{y}(\lambda_i)$, and $\bar{z}_i \equiv \bar{z}(\lambda_i)$ denote the values of the color matching functions for the three specific wavelengths λ_i.

The corresponding chromaticity coordinates that represent the color perceived by the eye are then calculated as a function of the addressed gray level vector from the normalization of the tristimulus values as

$$x(\hat{g}) = \frac{X(\hat{g})}{X(\hat{g}) + Y(\hat{g}) + Z(\hat{g})}, \tag{11a}$$

$$y(\hat{g}) = \frac{Y(\hat{g})}{X(\hat{g}) + Y(\hat{g}) + Z(\hat{g})}, \tag{11b}$$

$$z(\hat{g}) = \frac{Z(\hat{g})}{X(\hat{g}) + Y(\hat{g}) + Z(\hat{g})}. \tag{11c}$$

Therefore, the color gamut that can be generated is controlled via the three addressed gray levels, each $\hat{g}$

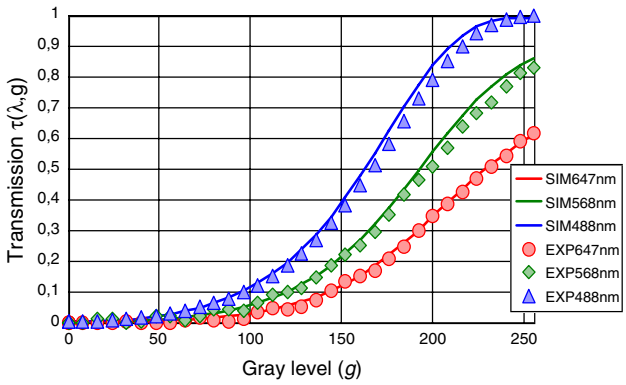

Fig. 4. (Color online) Intensity transmission of the TNLCD in the configuration ($\varphi_1 = 42°$,$\varphi_2 = -48°$) as a function of the addressed gray level for the RGB wavelengths. Continuous lines denote the numerically simulated prediction, while points denote the corresponding experimental data.

defining a point $[x(\hat{g}), y(\hat{g})]$ in the CIE*xy* chromaticity diagram. In Fig. 5, we mark the triangle defining the possible color gamut that can be generated using the Ar–Kr RGB monochromatic lines (647, 568, and 488 nm).

4. Experimental Results

Experimental evidence of the ability of the proposed setup for color tuning is provided here. Figure 6 shows the results derived from the transmittance curves in Fig. 4. We report the measured transmittance spectrum for specific values of the gray level vector $\hat{g} = (g_R, g_G, g_B)$. Figure 6(a) corresponds to the spectrum in Fig. 2(b) and can be considered as the reference white with relative weights $(1, 1, 1)$ in the RGB components. The other cases show the measured spectra when the addressed gray levels are adjusted in each of the three areas of the TNLCD to provide specific weights. For instance, in Figs. 6(b) and 6(c) the B and G lines are reduced simultaneously to achieve relative weights $(1/2, 1/2, 1)$ and $(0, 0, 1)$, providing a pink and a red recombined beam. Analogously, Figs. 6(d), 6(e), 6(f), and 6(g) show the measured spectra when the relative weights of the corresponding BGR lines are adjusted to be $(1/2, 1, 1/2)$, $(0, 1, 0)$, $(1, 1/2, 1/2)$ and $(1, 0, 0)$, respectively. In all cases, pictures of the output beam are also included as insets.

Figure 7 shows a numerical simulation of the points in the CIE*xy* diagram, which corresponds to the selection of different relative weights of the RGB lines in order to produce three different trajectories in the color chart. The origin of each color trajectory corresponds to the equally intense lines in Fig. 6(a). The three color diagrams in Fig. 7 correspond to three different sequences where the transmittances of two spectral lines are gradually decreased in steps of 10% at the same time. The addressed gray levels required to produce the selected transmittance in each line are calculated using the data in Fig. 4. For each case, the corresponding point $[x(\hat{g}), y(\hat{g})]$ is marked in the corresponding CIE*xy* chromaticity

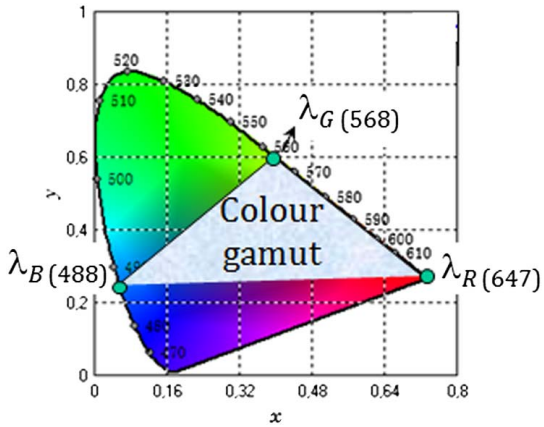

Fig. 5. (Color online) Color representation on the CIE*xy* chromaticity diagram of the three Ar–Kr laser lines (488, 568, and 647 nm) and the possible color gamut that can be reproduced.

diagram as a solid color point. The trajectory towards red [Fig. 7(a)] is obtained by reducing GB components. Analogous trajectories toward green and blue are obtained by simultaneously reducing the RB components [Fig. 7(b)], and the RG components [Fig. 7(c)], respectively. Since the two components are gradually decreased by the same amount, all three trajectories are straight lines starting from the central white point and approaching the corresponding pure monochromatic color. Although the irradiance steps are selected to be constant (10% variation), note that the CIE*xy* diagram is not linear with respect to irradiance variations, thus providing a nonlinear representation of the points along each line in Fig. 7.

Figure 8 shows the experimental verification measured with the spectrometer. The three straight trajectories in the simulation of Fig. 7 are reproduced with very good fidelity. The main differences occur at the edges of the diagram, where the pure monochromatic colors should be placed. These points are not reached in this experimental data. The reason is some residual noise detected by the spectrometer that adds some color content and thus it reduces the chromatic purity. But these experimental results evidence the ability to provide the color gamut described in Fig. 5.

5. Conclusions

In summary, in this work we proposed an optical system to control the color of a multiline RGB Ar–Kr laser employing a commercial TNLCD display. The optical setup is simple and it is based on decomposing the multiline emission of the laser into its three spectral components (RGB components) and then changing the TNLCD transmittance modulation function on each color channel respectively. An inverse optical setup recombines the color channels to obtain a variable color laser beam. Although such optical architectures have several sources of efficiency losses (mainly diffraction losses at the two gratings and at the LCD), it can still be useful if the input power budget of the light source is enough in comparison with the detection rate. This is the case in many of the mentioned applications in optoelectronic image processing, or diffractive optics, where the input laser often must be attenuated to avoid saturation of the usual final CCD detector.

The application of a predictive physical model for the microscopic retardance parameters of the TNLCD is a key aspect of the work, since it allows finding the best configuration of the polarizers to modulate all three RGB components and accurately reproduce the desired output colors. Note that since the TNLCD transmittance modulation depends on the tunable and independent polarization modification in each color channel, the same optical setup can be used (by removing the output polarizer) to manipulate the polarization spectral properties of the incoming light beam.

We provide colorimetric measurements of the output beam in order to show the wide gamut of laser

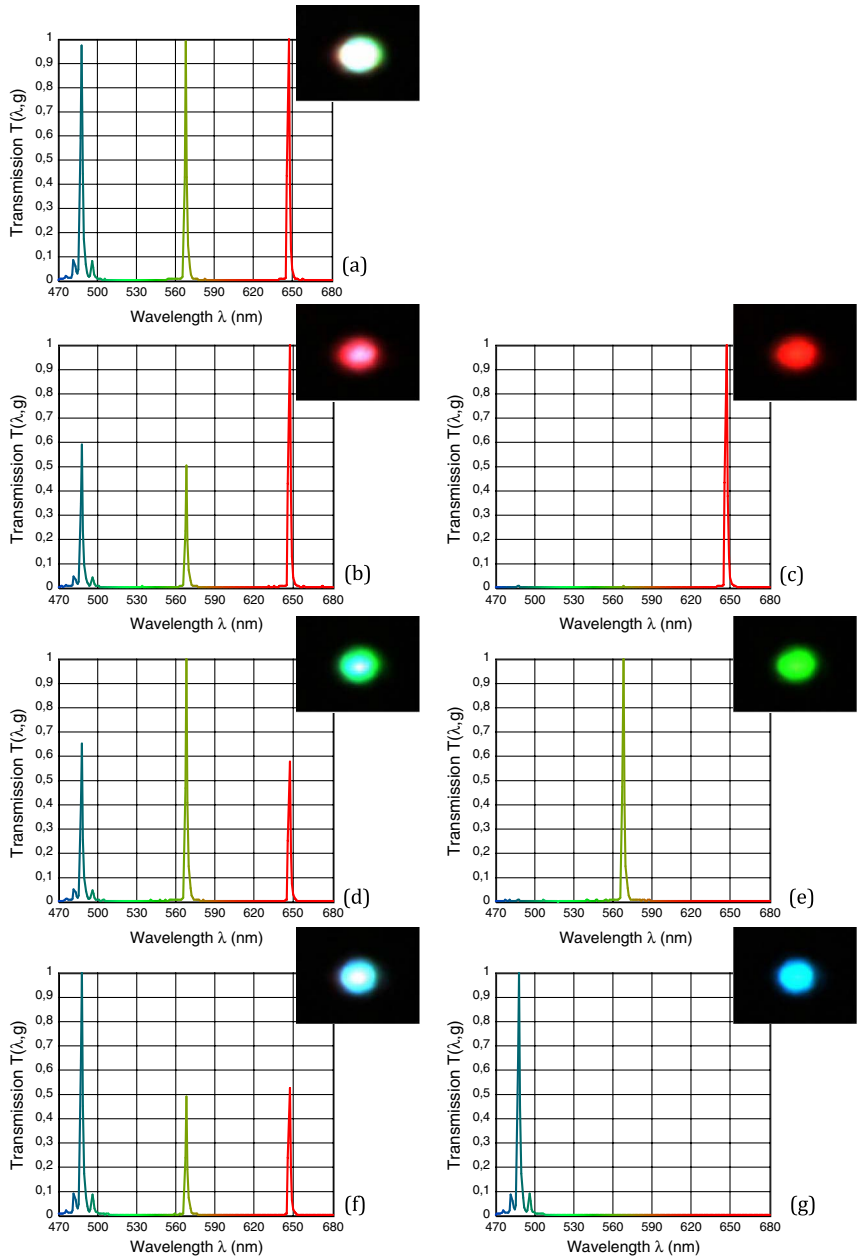

Fig. 6. (Color online) Experimental spectra and captured color output beam (as insets) for the relative weights of the spectral lines (BGR): (a) $(1,1,1)$; (b) $(1/2,1/2,1)$; (c) $(0,0,1)$; (d) $(1/2,1,1/2)$; (e) $(0,1,0)$; (f) $(1,1/2,1/2)$; and (g) $(1,0,0)$.

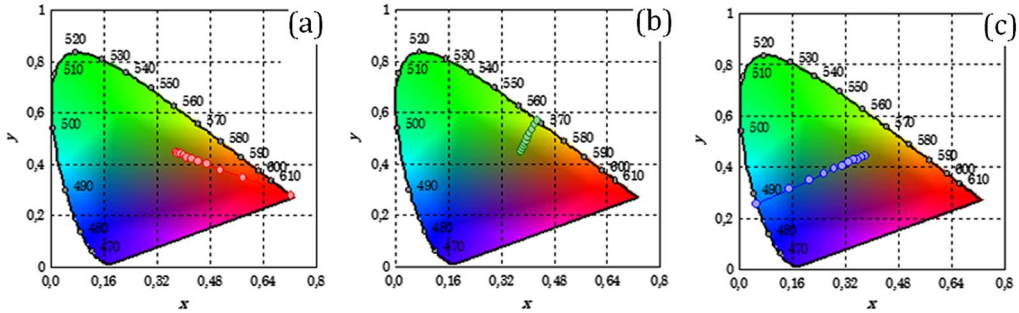

Fig. 7. (Color online) Simulation results for the representation in the CIE*xy* diagram of different sequences (solid color points) where, starting from three equally intense spectral lines, two of them are gradually decreased in steps of 10%. For each case the fully transmitted line is: (a) red, (b) green, or (c) blue.

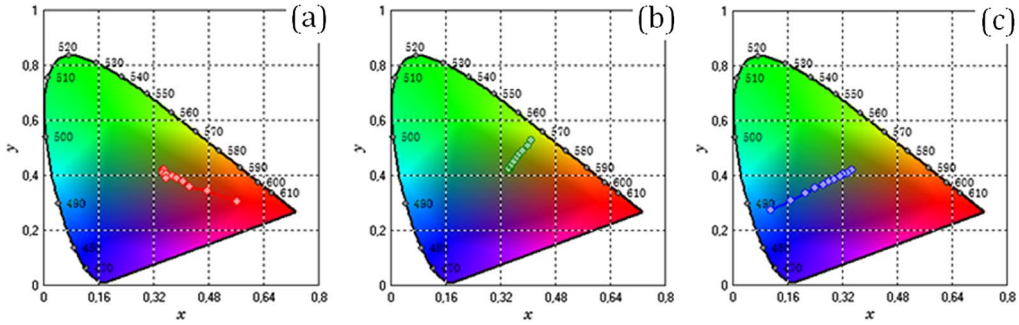

Fig. 8. (Color online) Experimental results corresponding to the simulation presented in Fig. 7.

colors that can be generated. The proposed system could be used in many applications where multicolor or polychromatic coherent sources are required with accurate tunable capacity, such as hyperspectral imaging systems or multicolor holography.

This work was supported by the Spanish Ministerio de Ciencia e Innovación (grants FIS2009-13955-C02-02 and 01). J. L. Martínez acknowledges a grant from Conselleria d'Educació i Ciència from Generalitat Valenciana.

References

1. P. Yeh and C. Gu, *Optics of Liquid Crystal Displays* (Wiley, 1999).
2. A. M. Pozo-Molina, J. J. Castro-Torres, and A. M. Rubiño-López, "Temporal stability and colour reproduction in fluorescent backlight LCD and AMOLED flat panel displays," Opt. Pura Apl. **43**, 207–212 (2010).
3. M. G. Robinson, J. Chen, and G. D. Sharp, "Color in projection displays," J. Display Technol. **1**, 118–124 (2005).
4. J. L. Martínez, A. Martínez-García, and I. Moreno, "Wavelength-compensated color Fourier diffractive optical elements using a ferroelectric liquid crystal on silicon display and a color-filter wheel," Appl. Opt. **48**, 911–918 (2009).
5. T.-L. Kelly and J. Munch, "Wavelength dependence of twisted nematic liquid crystal phase modulators," Opt. Commun. **156**, 252–258 (1998).
6. J. L. Martínez, P. García-Martínez, M. M. Sánchez-López, and I. Moreno, "Accurate colour predictability based on a spectral retardance model of a twisted-nematic liquid crystal display," Opt. Commun. **284**, 2441–2447 (2011).
7. P. J. Miller and C. C. Hoyt, "Multispectral color capture using a liquid crystal tunable filter," Opt. Eng. **41**, 2532–2548 (2002).
8. M. A. López-Álvarez, J. Hernández-Andrés, J. Romero, and R. L. Lee, "Designing a practical system for spectral imaging of skylight," Appl. Opt. **44**, 5688–5695 (2005).
9. M. S. Millán, J. Otón, and E. Pérez-Cabré, "Dynamic compensation of chromatic aberration in a programmable diffractive lens," Opt. Express **14**, 9103–9111 (2006).
10. A. M. Weiner, "Ultrafast optical pulse shaping: A tutorial review," Opt. Commun. **284**, 3669–3692 (2011).
11. D. J. Funk and D. S. Moore, "Fourier-transform spectroscopy using liquid crystal technology," Opt. Lett. **22**, 1799–1801 (1997).
12. S. V. Kartalopoulus, *Introduction to DWDM Technology* (SPIE, 2000).
13. D. Sinefeld, C. R. Doerr, and D. M. Marom, "A photonic spectral processor employing two-dimensional WDM channel separation and a phase LCoS modulator," Opt. Express **19**, 14532–14541 (2011).
14. Y. Zhang, H. Dong, R. Wang, J. Duan, A. Shi, Q. Fang, and Y. Liu, "Demonstration of a home projector based on RGB semiconductor lasers," Appl. Opt. **51**, 3584–3589 (2012).
15. Y. Saito, N. Nakai, A. Nomura, and T. Kano, "Spectral characteristics of a short-pulse red–green–blue dye mixture laser," Appl. Opt. **31**, 4298–4304 (1992).
16. T. Kampfe, E. Kley, A. Tunnermann, and P. Dannberg, "Design and fabrication of stacked, computer generated holograms for multicolor image generation," Appl. Opt. **46**, 5482–5488 (2007).
17. D. Brotherton-Ratcliffe, S. J. Zacharovas, R. J. Bakanas, J. Pileckas, A. Nikoskij, and J. Kuchin, "Digital holographic printing using pulsed RGB lasers," Opt. Eng. **50**, 091307 (2011).
18. T. Shimonaba and T. Ito, "A color holographic reconstruction system by time division multiplexing with reference lights of laser," Opt. Rev. **10**, 339–341 (2003).
19. T. Shimonaba, A. Shiraki, N. Masuda, and T. Ito, "An electroholographic color reconstruction by time division switching of reference lights," J. Opt. A Pure Appl. Opt. **9**, 757–760 (2007).
20. A. Márquez, C. Iemmi, I. Moreno, J. A. Davis, J. Campos, and M. J. Yzuel, "Quantitative prediction of the modulation behaviour of twisted nematic liquid crystal displays based on a simple physical model," Opt. Eng. **40**, 2558–2564 (2001).
21. I. Moreno, A. M. Cutillas, M. M. Sánchez-López, P. Velásquez, and F. Mateos, "Full prediction of the broadband optical modulation performance of a twisted nematic liquid crystal cell," Opt. Commun. **281**, 5520–5526 (2008).
22. A. Lizana, A. Márquez, I. Moreno, C. Iemmi, J. Campos, and M. J. Yzuel, "Wavelength dependence of polarimetric and phase-shift characterization of a liquid crystal on silicon display," J. Eur. Opt. Soc. Rapid Pub. **3**, 08011 (2008).
23. D. Malacara, *Color Vision and Colorimetry* (SPIE, 2002).